Role of hypercooling limit in supercooling behavior and glass formation

Lei Wang [1], Yong Chan Cho [1], Yun-Hee Lee [1], Sangho Jeon [2], and Geun Woo Lee [1,3,*]

[1] *Frontier of Extreme Physics, Korea Research Institute of Standards and Science, 209 Gajeong-Ro, Yuseong-Gu, Daejeon 34113, Republic of Korea*

[2] *Deutsches Elektronen-Synchrotron (DESY), Notkestraße 85, D-22607 Hamburg, Germany*

[3] *Applied Measurement Science, University of Science and Technology (UST), 217 Gajeong-Ro, Yuseong-Gu, Daejeon 34113, Republic of Korea*

(Received 10 March 2024; accepted 13 May 2024; published 3 June 2024)

Supercooling of liquids is a crucial phenomenon to understand and control crystallization and vitrification in various research fields. In particular, deep supercooling beyond a certain limit, called hypercooling, is practically important for manipulating glass formation as well as crystal nucleation and growth. However, it is still very ambiguous how hypercooling occurs and impacts glass formation. In this work, we find that the hypercooling behavior of liquids is determined by the combination of undercoolability and hypercoolability, unlike the common belief that deep supercooling is the prerequisite to observe hypercooling. This provides an answer to a long-standing question of why certain materials exhibit hypercooling behavior, even though their liquids only have small degree of supercooling. Moreover, we find a clear connection between the hypercooling limit and glass forming ability, which explicitly reveals the hidden role of the hypercooling limit in glass formation from both thermodynamic and kinetic viewpoints. The present results provide not only a key parameter for materials design but also an insight into understanding glass formation.

DOI: 10.1103/PhysRevMaterials.8.063401

I. INTRODUCTION

The discovery of the deep supercooling phenomenon [1] has attracted considerable attention for its fundamental understanding and industrial application in many research areas. In particular, the deep supercooling of metallic liquids has led to remarkable discoveries and questions about nucleation and vitrification, such as the local order of liquid metals [2], negentropy phenomenon at the crystal-liquid interface [3], glass formation mechanism [4–7], nonequilibrium crystal growth [8], and bulk metallic glasses (BMGs) [9,10]. When liquid supercools below its melting temperature, the driving force for crystallization increases. Thus, the liquid finally crystallizes, releasing latent heat which increases the temperature back to the melting point (called recalescence). If the liquid is partially crystallized during the recalescence, the remaining liquid crystallizes at the melting temperature, forming a plateau [path ① in Fig. 1(a)]. When the supercooled liquid deeply cools below a critical temperature known as hypercooling limit (T_{hyp}), it completely crystallizes during recalescence, showing no plateau [path ② in Figs. 1(a) and 1(b)]. The former behavior is called hypocooling, the latter hypercooling. The hypercooling behavior of liquids has been intensively investigated in crystal growth studies, since it produces various nonequilibrium crystal growth phenomena during solidification [11–16], affecting the mechanical properties of materials.

Moreover, hypercooling behavior has also been an important precursor to glass formation in metallic alloys and oxides [17,18]. Recent studies indicate that $Cu_{50}Zr_{50}$ liquid forming a BMG exhibits slow kinetics of crystal growth when cooled below the T_{hyp} [12,19,20]. In addition, many liquids forming good BMGs have also displayed hypercooling behavior [21,22]. Interestingly, early transition metal (ETM) liquids with hypercooling behavior [23,24] have shown better glass forming ability (GFA) [25,26] than late transition metal (LTM) liquids with hypocooling behavior [23].

However, the relations between the hypercooling limit, maximum undercooling, and GFA are still unclear to date. For example, ETM liquids, despite exhibiting lower undercoolability than most LTM liquids [23,27], exhibit hypercooling behavior and relatively easier glass formation. This seems counterintuitive, since hypercooling is generally considered as the result of deep supercooling. Furthermore, some good BMGs have also shown smaller undercoolability than elements and alloys [21,28], highlighting the ambiguity of the relationship between the hypercooling limit, the degree of supercooling, and GFA. Until now, most GFA parameters have been developed with melting temperature (T_m), glass transition temperature (T_g), crystallization temperature (T_x) upon heating, and enthalpy (or density) difference between crystal and glass [29,30], but no T_{hyp} or ΔT_{hyp} ($= T_m - T_{hyp}$). Thus, the explicit connections among the hypercooling limit, degree of supercooling, and glass formation should be addressed with essential parameters governing the hypercooling behavior.

In this work, we provide a perspective to understand the occurrence of hypercooling behavior and its role in glass

*Corresponding author: gwlee@kriss.re.kr

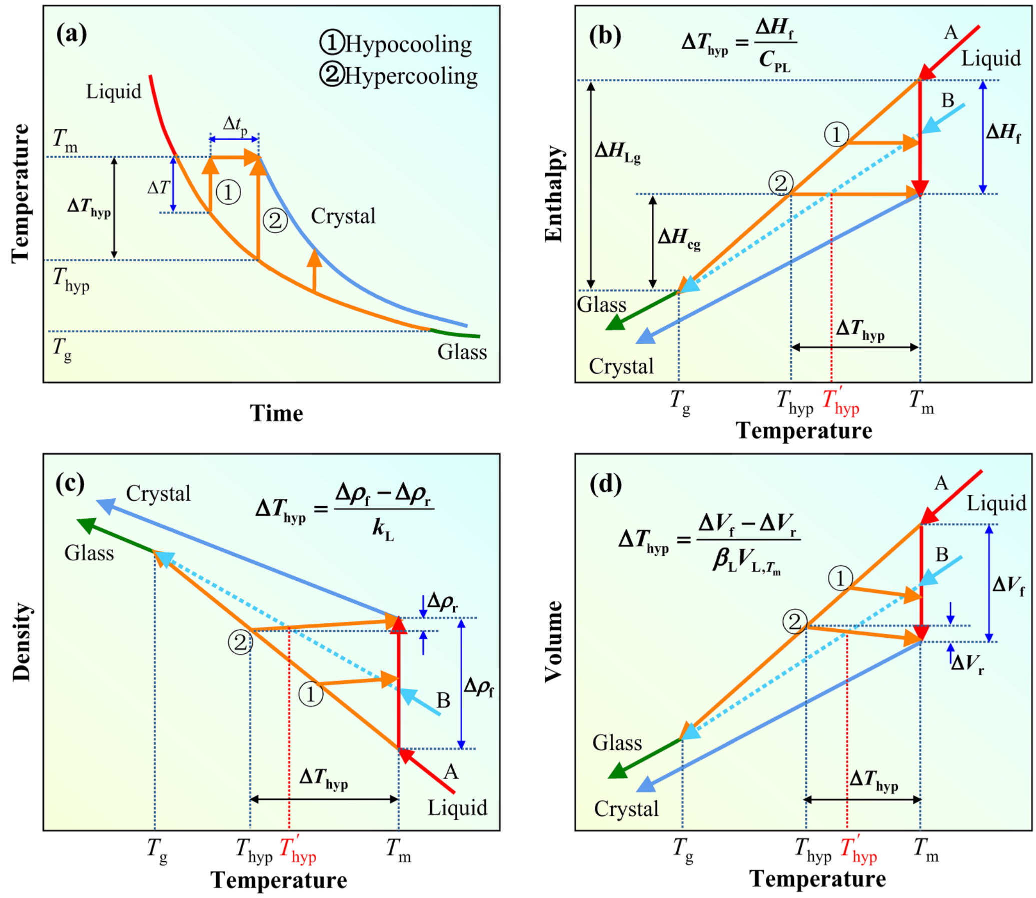

FIG. 1. Cooling process of a liquid showing various supercooling behaviors under adiabatic conditions: (a) Temperature-time curves; in hypocooling behavior (path ①), the supercooled liquid solidifies through the nonequilibrium condition during recalescence and equilibrium condition during plateau regime; in hypercooling behavior (path ②), the supercooled liquid solidifies completely during recalescence. (b) Enthalpy-temperature curves; T_{hyp} is a temperature where the enthalpy of liquid is equal to that of crystal at the melting temperature T_m, and $\Delta T_{hyp} = T_m - T_{hyp}$ is the hypercooling limit. (c), (d) Density and volume-temperature curves. Since crystallization is not an isochoric process, there is a volume change ΔV_r (density change $\Delta\rho_r$) during recalescence. Alloying effect (A → B) is conceptually illustrated in (b), (d). β_L $(= -dV_L/dT/V_{L,Tm})$ in (d) is the volumetric thermal expansion coefficient of liquids.

formation. Remarkably, we find that hypercooling behavior is determined by the combination of undercoolability U_{max} $(= \Delta T_{max}/T_m)$ and hypercoolability U_{hyp} $(=\Delta T_{hyp}/T_m)$ which can be described by a dimensionless parameter $\alpha_{hyp}[= U_{max}/U_{hyp} > 1$ (hypercooling), and <1 (hypocooling)]. This means that hypercooling behavior can occur even with small ΔT_{max}, particularly when U_{hyp} is smaller than U_{max}. In other words, deep supercooling is not the only prerequisite for achieving hypercooling. In particular, we clearly demonstrate that the hypercooling behavior of binary alloy liquids occurs due to the combination of these two quantities. Moreover, we establish a direct link between the hypercooling parameter (α_{hyp}) and the GFA across binary to multicomponent BMGs. This relationship can be explained by the thermodynamic and kinetic viewpoints of classical nucleation theory (CNT). Accordingly, these results will provide a new insight into understanding the relationship between hypercooling, supercooling, and glass formation, as well as give a strong impact on tailoring alloy design since we have one more degree of freedom to control the supercooling behavior (i.e., through U_{hyp}).

II. MATERIALS AND METHODS

Spherical samples were prepared with high-purity elemental materials (all >99.9% purity, Alfa Aesar) [31] by arc-melting under a protective Ar atmosphere (99.9999% purity). A zirconium ingot was melted to remove the residual oxygen in the chamber before processing the samples. The samples were flipped and remelted at least four times to ensure the uniformity of the alloy composition, and the mass loss due to arc-melting was checked to be less than 0.2% of the initial mass.

Supercooling and density measurements of the samples were performed by a high vacuum electrostatic levitation (ESL) facility ($\sim 10^{-7}$ Torr), built at the Korea Research Institute of Standards and Science (KRISS) [31–33]. ESL provides a containerless environment which minimizes heterogeneous nucleation sites from the container walls, substantially enhancing supercooling [24] and promoting glass formation [17,21].

During experiments, a levitated sample (2 mm in diameter) is heated and melted using three lasers (UNIVERSAL, ULCR-100) which have equal power and slightly larger beam size than the sample, and are symmetrically aligned. This configuration minimizes temperature gradients on the sample and translational or rotational sample motion, ensuring deep supercooling and precise density measurement [33]. The sample temperature is continuously monitored by three infrared pyrometers (CHINO IR-CAI with 1.55 µm wavelength, METIS MI16 with 1.6 µm wavelength, and CHINO IR-CAS with 0.9 µm wavelength), calibrated with the melting temperature (for pure elements and binary alloys, refer to the data in the phase diagram [34]; for ternary and multicomponent glass-forming alloys, as determined by differential scanning calorimetry (DSC) (Setaram Instrumentation, LABSYS evo) measurements). The density measurement is conducted by an imaging method with the combination of UV background light (LICHTZEN Inno-cure 5000) and a black-white CCD camera (BASLER piA640-210 gm). Before measurements, several melting-solidification cycles are performed to ensure deep and consistent supercooling levels. The maximum supercooling $\Delta T_{\max}$ achieved is taken as intrinsic undercoolability $U_{\max}$ $(= \Delta T_{\max}/T_{\mathrm{m}})$. The density of metallic liquids is then measured during the radiative cooling process, covering a wide range of stable and supercooled temperatures. This ESL technique provides high accuracy in density measurement for high-temperature materials. Detailed information on the instrument, experimental procedures, and uncertainty evaluation of density measurement can be found in our previous studies [31–33].

III. RESULTS AND DISCUSSION

A. Determination of hypercooling and its mechanism on elemental liquids

1. New determination of hypercooling limit

Crystallization from hypercooling temperature occurs via the isenthalpic process during recalescence [Figs. 1(a)-② and 1(b)-②]. Thus, the released heat during recalescence should be the same as fusion enthalpy, establishing a relationship between the hypercooling limit (ΔT_{hyp}) and fusion enthalpy (ΔH_{f}): $\Delta T_{\mathrm{hyp}} = T_{\mathrm{m}} - T_{\mathrm{hyp}} = \Delta H_{\mathrm{f}}/C_{\mathrm{P,L}}$ [35]. However, measuring the specific heat $C_{\mathrm{P,L}}$ and ΔH_{f} is often challenging for high-temperature metallic melts and is usually obtained separately, causing significant uncertainty [36], and is time consuming. Thus, we provide an alternative way to determine ΔT_{hyp} with density or volume measurements, which can be carried out efficiently and precisely by using ESL.

Unlike the isenthalpic process during recalescence [Fig. 1(b)], density increases upon crystallization (i.e., this is not an isochoric process [Fig. 1(c)]. The total density difference ($\Delta\rho_{\mathrm{f}}$) between the liquid and crystal phases at T_{m} is described by Eq. (1) under the hypercooling condition

$$\Delta\rho_{\mathrm{f}} = \Delta\rho_{l} + \Delta\rho_{\mathrm{r}}, \quad (1)$$

where $\Delta\rho_{l}$ represents the density change of the supercooled liquid from T_{m} to T_{hyp} and $\Delta\rho_{\mathrm{r}}$ is the density change during recalescence. Therefore, the hypercooling limit ΔT_{hyp} is given by

$$\Delta T_{\mathrm{hyp}} = \frac{\Delta\rho_{\mathrm{f}} - \Delta\rho_{\mathrm{r}}}{k_{\mathrm{L}}}, \quad (2)$$

where $k_{\mathrm{L}} = -d\rho_{\mathrm{L}}/dT$ is the temperature coefficient of liquid density at T_{m} [see also volume expression in Fig. 1(d)]. As exhibited in Fig. 2(b), these independent parameters can be obtained simultaneously through density measurement during the cooling process, covering regions from supercooled liquids to crystallized solids, using ESL [31]. In addition, Figs. 1(b)–1(d) show that ΔT_{hyp} decreases when ΔH_{f}, ΔV_{f}, and $\Delta\rho_{\mathrm{f}}$ become smaller by alloying (marked by B). Thus, the liquid easily approaches T_{hyp} with small supercooling, slowing down the kinetics of atomic motion and increasing the possibility of glass formation, as we will show later.

2. Effect of density difference between liquid and crystal on hypercooling phenomenon; elemental metallic liquids

As shown in Eq. (2), we first examine the relation of ΔT_{hyp} and $\Delta\rho_{\mathrm{f}}$ with twelve elemental liquids. Figure 2 shows representative hypocooling and (quasi)hypercooling behaviors in temperature-time (T-t) curves and density data as depicted in Figs. 1(a) and 1(c) [see other elements in Fig. S1 in the Supplemental Material (SM) [37], see also Refs. [38–62] therein]. The respective $\Delta\rho_{\mathrm{f}}$, $\Delta\rho_{\mathrm{r}}$, and k_{L} values of various elements are deduced from their density data (see details in Fig. S1(b) and Table S1 in SM [37]). In Figs. 2(a) and 2(b), we observe that quasihypercooling behavior of ETMs (e.g., Ti, Zr, Hf) gradually changes into hypocooling behavior of LTMs (e.g., Ni, Pd, Pt) with an obvious plateau after recalescence (see all the T-t curves of elemental liquids in Fig. S1(a) in SM [37]).

The deduced ΔT_{hyp} and U_{hyp} $(= \Delta T_{\mathrm{hyp}}/T_{\mathrm{m}})$ based on Eq. (2) are given in Fig. 2(c) and Table I. The ΔT_{hyp} values agree well with those obtained by the zero-plateau time (ZPT) method [35,63–65], which is a typical method to determine ΔT_{hyp} (see ΔT_{hyp} (ZPT) determination in Fig. S2 in SM [37]). Interestingly, $\Delta\rho_{\mathrm{f}}$, $\Delta\rho_{\mathrm{r}}$, and k_{L} values roughly increase with atomic number Z in the same period, and these values are larger in fcc LTMs than in bcc ETMs overall [Figs. 2(d), 2(e), and 2(f)]. Note that the quasihypercooling behavior in ETM liquids is observed, regardless of their small $\Delta\rho_{\mathrm{r}}$ and k_{L} values [Figs. 2(e) and 2(f)]. This implies that hypercooling behavior is dominated by $\Delta\rho_{\mathrm{f}}$. In addition, ΔT_{hyp} (and U_{hyp}) of Ti, Zr, and Hf is smaller than that of Ni, Pd, and Pt [Fig. 2(c) and Table I]. This can be understood by smaller $\Delta\rho_{\mathrm{f}}$ [Fig. 2(d)]. That is, the packing density Φ of ETM crystals with bcc structure ($\Phi = 0.68$ at 0 K, and $\Phi = 0.62$ at T_{m} [66]) is smaller than that of LTM crystals with fcc structure ($\Phi = 0.74$ at 0 K, and $\Phi = 0.66$ at T_{m} [66]), while the packing densities of the ETM and LTM liquids are almost same at T_{m} ($\Phi \sim$ 0.44–0.46 [67]). Therefore, ETMs have smaller $\Delta\rho_{\mathrm{f}}$ than LTMs due to their crystal structure differences, explaining the smaller ΔT_{hyp} in ETMs than in LTMs along the same period. Moreover, the smaller ΔT_{hyp} might contribute to the easier glass formation of ETMs than LTMs [25,26], if the ΔT_{hyp} is strongly correlated with GFA.

Another interesting point is that the ETMs (i.e., Ti, Zr, and Hf) showing the quasihypercooling behavior do not exhibit the largest undercoolability $U_{\max}$ among the liquids in present ESL experiments [Fig. 2(c) and Table I]. This is somewhat counterintuitive based on Fig. 1, since it has been commonly believed that hypercooling is the result of maximum supercooling. We should note that the ΔT_{hyp} is an intrinsic

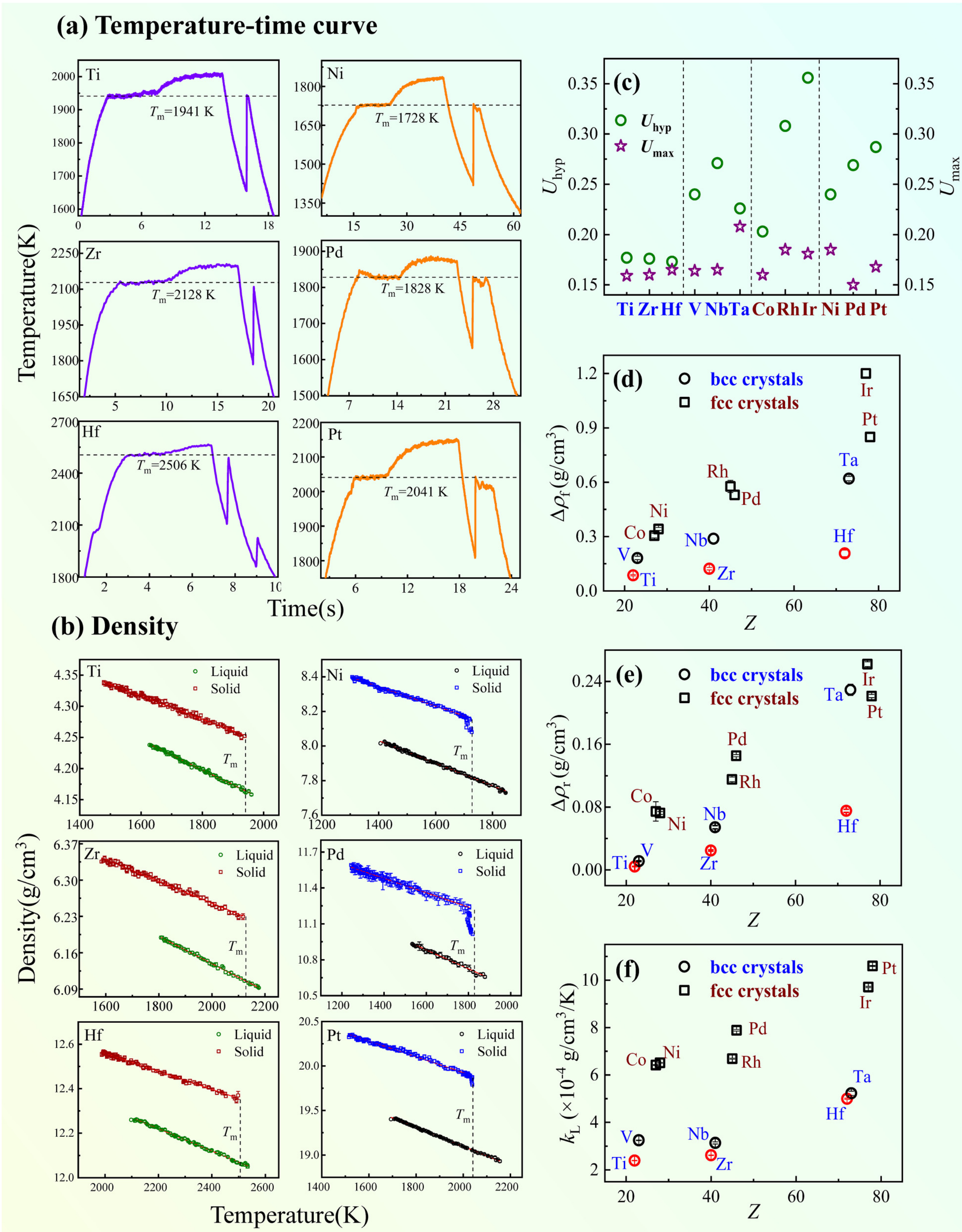

FIG. 2. (a) Typical temperature-time (T-t) profile and (b) density property of ETMs and LTMs measured by ESL. Figures are arranged in the order of periodic table. The quasihypercooling and hypocooling behaviors are represented by violet and orange colors in T-t curves, respectively; (c) $U_{\mathrm{hyp}}(=\Delta T_{\mathrm{hyp}}/T_{\mathrm{m}})$ and U_{max} $(=\Delta T_{\mathrm{max}}/T_{\mathrm{m}})$; (d) density difference $(\Delta\rho_{\mathrm{f}})$ between liquid and crystal at T_{m}; (e) density change during recalescence $\Delta\rho_{\mathrm{r}}$; (f) temperature coefficient of liquid density k_{L} of ETMs and LTMs.

TABLE I. Supercooling and hypercooling properties of elemental metallic liquids.

Elements	T_m (K)	ΔT_{max} (K)	U_{max}	ΔT_{hyp} (K) (density)	ΔT_{hyp} (K)[a] (ZPT)	U_{hyp}	α_{hyp}[b]
Ti (bcc)	1941	308	0.159	344	$344 \pm 5/341 \pm 5$ [63]	0.177	0.895
V (bcc)	2183	357	0.164	524	556 ± 20	0.240	0.681
Zr (bcc)	2128	340	0.160	375	$374 \pm 10/374 \pm 5$ [23]	0.176	0.907
Nb (bcc)	2750	455	0.165	744	$730 \pm 30/641 \pm 10$ [23]/706 [64]	0.271	0.612
Hf (bcc)	2506	413	0.165	433	$404 \pm 15/399$ [23]	0.173	0.954
Ta (bcc)	3290	683	0.208	744	784 ± 30	0.226	0.918
Co (fcc)	1766	283	0.160	358	375 ± 15	0.203	0.791
Ni (fcc)	1728	320	0.185	414	$423 \pm 15/410$ [65]/444 ± 5 [23]	0.240	0.773
Rh (fcc)	2237	414	0.185	689	$706 \pm 30/650 \pm 10$ [23]	0.308	0.601
Pd (fcc)	1828	274	0.150	491	465 ± 25	0.269	0.558
Ir (fcc)	2719	493	0.181	969	984 ± 35	0.356	0.509
Pt (fcc)	2041	343	0.168	586	624 ± 30	0.287	0.585

[a]The errors express standard deviation (SD).
[b]α_{hyp} of bcc ETMs on Ti, Zr and Hf demonstrating quasihypercooling is close to 1 and larger than that of fcc LTMs on Ni, Pd, and Pt exhibiting hypocooling behavior.

property of materials determined by the density and thermal expansion coefficient, or fusion enthalpy and specific heat (i.e., $(\Delta\rho_f - \Delta\rho_r)/k_L$ or $\Delta H_f/C_{P,L}$), while the supercooling ΔT_{max} is governed by the stability of the supercooled liquids [68]. This provides a new perspective that the hypercooling behavior can be manipulated by reducing the hypercooling limit (ΔT_{hyp}), as we will demonstrate in alloy cases.

B. Competition of hypercooling limit and maximum supercooling affecting the supercooling behavior; binary alloy liquids

As we recognize in Fig. 1(a), the hypercooling behavior of the supercooled liquid can be manipulated by either increasing ΔT or decreasing ΔT_{hyp}. When we mix two different kinds of atoms to form alloys, density properties (i.e., $\Delta\rho_f$, $\Delta\rho_r$, and k_L) and Gibbs free energy of the alloy liquids vary from their elemental properties, changing the ΔT_{hyp} and the ΔT_{max}, respectively. The origin of the hypercooling behavior should be distinguished by the impact of ΔT_{hyp} or ΔT_{max}. Thus, we here introduce a parameter α_{hyp} to discern the supercooling behavior

$$\alpha_{hyp} = \frac{\Delta T_{max}}{\Delta T_{hyp}} = \frac{U_{max}}{U_{hyp}}. \quad (3)$$

$\alpha_{hyp} \geqslant 1$ means the hypercooling case, while $\alpha_{hyp} < 1$ denotes the hypocooling one.

We investigate the role of U_{max} and U_{hyp} in supercooling behaviors with nine miscible binary alloys having bcc and fcc structures, as well as six binary intermetallic compounds. In Fig. 3, $Ti_{50}Zr_{50}$, $Zr_{50}Hf_{50}$, $Co_{50}Pd_{50}$, $Ni_{50}Ti_{50}$, $Ni_{50}Hf_{50}$, and $Cu_{50}Zr_{50}$ alloys show evident hypercooling behavior, while other alloys do hypocooling (see detailed density data, U_{max}, and U_{hyp} as well as their deviations caused by mixing in Fig. S3 and Table S2-S3 in SM [37]). Surprisingly, we find that alloying unequally influences U_{max} and U_{hyp} so that the hypercooling behavior of binary alloy liquids has different origins as shown in Fig. 4.

1. *bcc miscible alloys* ($\Delta H_{mix} = 0$)

We first consider a simple case with the bcc miscible alloy system (e.g., $Ti_{50}Zr_{50}$ and $Zr_{50}Hf_{50}$) having zero mixing enthalpy ΔH_{mix} [38]. In this case, alloying modifies density and only mixing entropy ΔS_{mix} in ΔG_{mix} (i.e., $\Delta G_{mix} = \Delta H_{mix} - T\Delta S_{mix}$). After alloying, the U_{max} of $Ti_{50}Zr_{50}$ alloy slightly increases by 4.70% from the average values of the elements, while little change is observed in the U_{max} of $Zr_{50}Hf_{50}$ alloy [see $\delta(U_{max})$ in Fig. 4(c)]. On the other hand, the change of hypercooling limit [i.e., $\delta(U_{hyp})$] shows relatively large reductions of 9.92% for $Ti_{50}Zr_{50}$ and 11.75% for $Zr_{50}Hf_{50}$, compared to their $\delta(U_{max})$ in Fig. 4(c). Thus, the smaller U_{hyp} than U_{max} gives $\alpha_{hyp} > 1$ [Figs. 4(a) and 4(b)], corresponding to the hypercooling behavior in Fig. 3 (a). As we expected in Eq. (2), the reduced $\Delta\rho_f$ with −13.87% for $Ti_{50}Zr_{50}$ and −13.03% for $Zr_{50}Hf_{50}$ is the main source for the large decreasing U_{hyp}, with relatively small changes of $\delta(k_L)$ by alloying [Fig. 4(d)]. Thus, the hypercooling in these bcc miscible alloys mainly originates from the reduced hypercoolability (U_{hyp}).

2. *fcc miscible alloys* ($\Delta H_{mix} \sim 0$)

We observe more notable supercooling behavior in fcc miscible alloy liquids. Among the fcc miscible alloy liquids in this study, $Co_{50}Pd_{50}$ is the only alloy exhibiting hypercooling behavior [Fig. 3(a)]. This is very interesting, because Co and Pd have shown hypocooling behavior like other LTMs in Fig. S1(a) [37]. In this case, alloying increases U_{max} by 43.23% and reduces U_{hyp} by 17.20% from the average values of its constituents (i.e., Co and Pd) [Fig. 4(c)]. This synergetic effect yields the highest α_{hyp} value (1.137) among the binary alloys in this study [Fig. 4(b)]. Again, it is worth mentioning that the large reduction of U_{hyp} in $Co_{50}Pd_{50}$ is ascribed to a remarkable reduction in $\Delta\rho_f$ of 29.78% and an increase in k_L of 16.95% [Fig. 4(d)].

We further investigate the effect of constituents on the hypercooling behavior of $Co_{50}Pd_{50}$ liquid by replacing Co with Fe and Ni. Since Fe and Ni have almost the same atomic

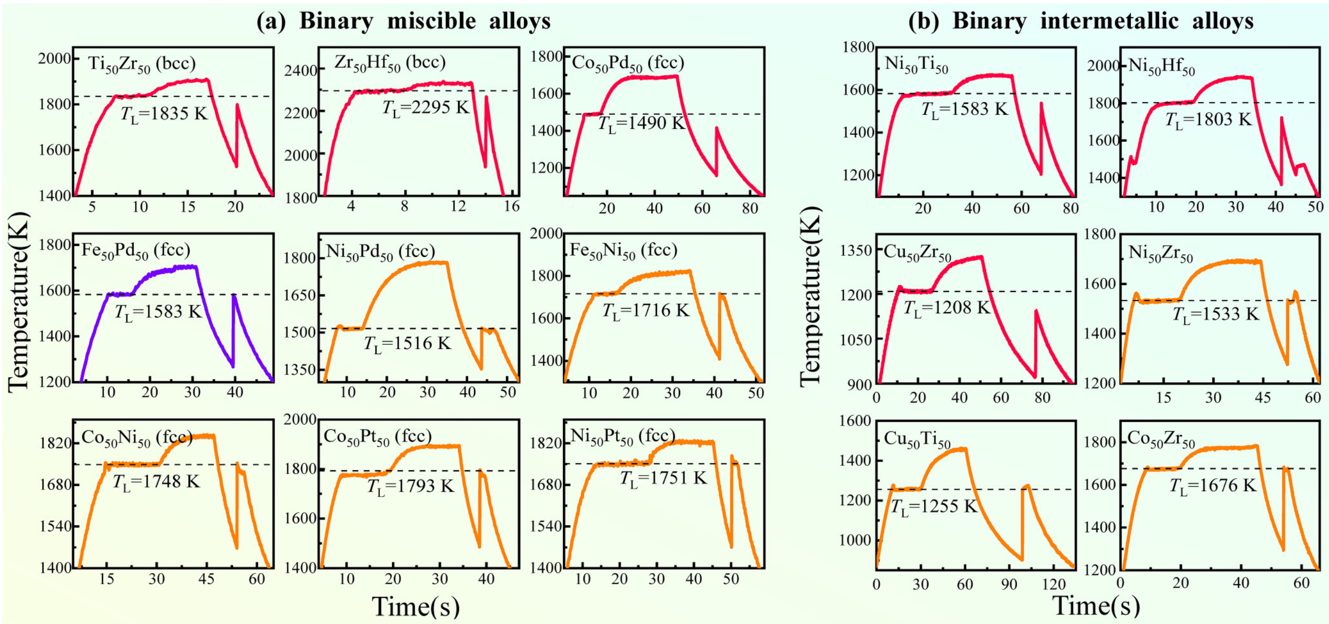

FIG. 3. Supercooling behaviors of various binary alloy liquids (a) miscible and (b) intermetallic compound alloy liquids. The hyper-, quasihyper- and hypocooling behaviors are represented by red, violet, and orange colors, respectively.

size with Co [69] and similar $\Delta H_{\mathrm{mix}}(\sim 0)$ with Pd [38], their alloying with Pd expects similar supercooling behavior as in $Co_{50}Pd_{50}$. However, the supercooling behavior of $Fe_{50}Pd_{50}$ looks hypercooling [Fig. 3(a)], but actually, α_{hyp} is less than one, indicating hypocooling or quasihypercooling [Fig. 4(b)]. This is due to the smaller changes in U_{hyp} (−9.54%) and $U_{\max}$ (23.22%) of $Fe_{50}Pd_{50}$ liquid, compared with those of $Co_{50}Pd_{50}$ liquid [Fig. 4(c)].

In the case of $Ni_{50}Pd_{50}$ alloy, we find a large decrease of $\delta(U_{\mathrm{hyp}})$ (−35.04%) due to a significant reduction of $\Delta\rho_{\mathrm{f}}$ [Figs. 4(c) and 4(d)]. However, the $U_{\max}$ of $Ni_{50}Pd_{50}$ liquid yields the smallest value (0.11) in this study [Figs. 4(a) and 4(c)]. Thus, $Ni_{50}Pd_{50}$ liquid shows the hypocooling behavior with $\alpha_{\mathrm{hyp}} < 1$ [Figs. 3(a) and 4(b)]. This case clearly demonstrates that the hypercooling behavior of liquids is the result of the competition between their hypercoolability (U_{hyp}) and undercoolability ($U_{\max}$). Accordingly, the supercooling behavior of miscible alloy liquids is rather complicated, although they have similar atomic size and zero or small ΔH_{mix}. Moreover, the results with Pd-X (Fe, Co, Ni) liquids strongly reflect that the $U_{\max}$ and U_{hyp} of alloy liquids can be affected by their electronic interactions.

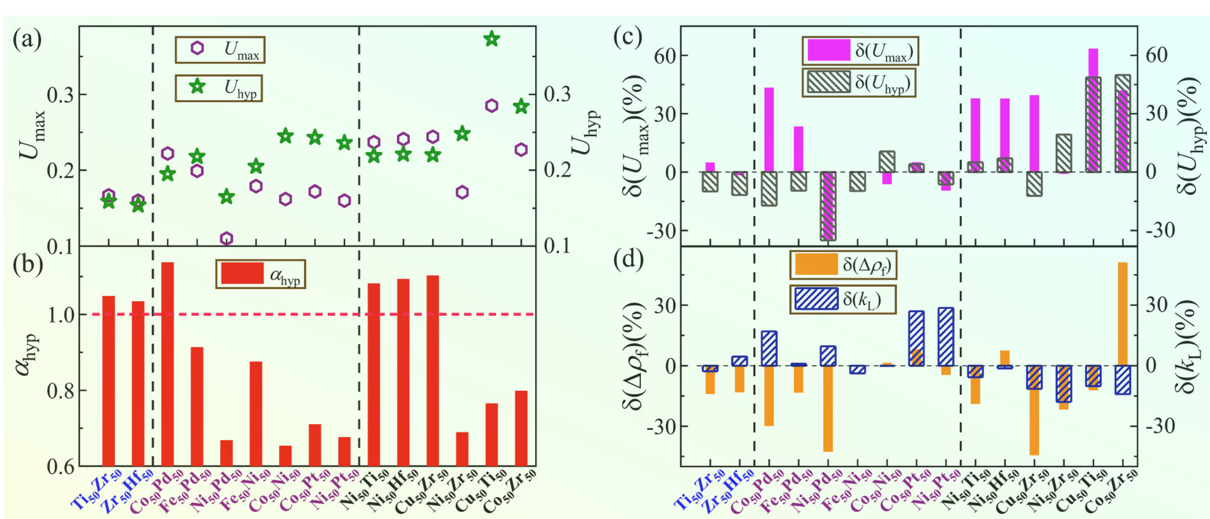

FIG. 4. Hypercooling origin on binary alloy liquids. (a) Experimentally determined $U_{\max}$, U_{hyp}; (b) α_{hyp} based on Eq. (3); (c), (d) Deviations of $U_{\max}$, U_{hyp} and $\Delta\rho_{\mathrm{f}}$, k_{L} from the average values of constituent elements caused by mixing. In (a)–(d), bcc, fcc and compound binary alloys are marked by blue, violet, and black colors, respectively.

3. Intermetallic compounds (large negative ΔH_{mix}*)*

We now consider more complex situations with intermetallic compounds, taking into account the ΔH_{mix} effect. In these cases, alloying yields a large negative ΔG_{mix} which may strongly stabilize the supercooled liquids [70], leading to large ΔT_{max} (or U_{max}). In addition, different atomic sizes might significantly change the packing efficiency of their liquids [71], resulting in the reduction of $\Delta\rho_f$ between their crystalline and liquid phases and thus ΔT_{hyp} (or U_{hyp}) too. Thus, we may anticipate hypercooling behavior with the intermetallic compound liquids.

We investigate six intermetallic alloy liquids and find the hypercooling behavior with three binary alloy liquids ($Ni_{50}Ti_{50}$, $Ni_{50}Hf_{50}$, and $Cu_{50}Zr_{50}$) [Figs. 3(b) and 4(b)]. For Ni-based alloys, the hypercooling behavior of $Ni_{50}Ti_{50}$ and $Ni_{50}Hf_{50}$ liquids results from a huge increase of ~38% in U_{max} mainly, comparing their average U_{max} of the constituents [Fig. 4(c)]. In contrast, $Ni_{50}Zr_{50}$ exhibits hypocooling behavior [Fig. 3(b)] due to a large increase in U_{hyp}, but almost no change in U_{max} [Fig. 4(c)].

$Cu_{50}Zr_{50}$ alloy liquid shows the hypercooling behavior due to the synergetic effect of U_{max} and U_{hyp} caused by a large increase of U_{max} (39.43%) and a huge decrease of U_{hyp} (12.18%). Unlike the case of $Co_{50}Pd_{50}$ liquid showing the same synergetic effect of the two factors, the large reduction of U_{hyp} of $Cu_{50}Zr_{50}$ liquid results from a negative change of k_L as well as a significant decrease of $\Delta\rho_f$ (−44.27%) [Figs. 4(c) and 4(d)].

Interestingly, the U_{max} of $Cu_{50}Ti_{50}$ liquid is even larger than that of $Cu_{50}Zr_{50}$ [Fig. 4(a)], which possibly prefers hypercooling. However, the highest U_{hyp} (0.373) offsets the benefit of large U_{max}, resulting in hypocooling behavior finally [Figs. 3(b) and 4(b)]. Similarly, the greatly enhanced U_{hyp} (49.87%) of $Co_{50}Zr_{50}$ prevents the hypercooling behavior, although its U_{max} also substantially increases by 41.88% after alloying [Fig. 4(c)]. It should be noted that the large ΔT_{hyp} (or U_{hyp}) of $Co_{50}Zr_{50}$ liquid results from the largest increase of $\Delta\rho_f$ on alloying, which is not observed in other alloy liquids in the present work.

These results clearly demonstrate that the supercooling behavior of the intermetallic liquids is determined by the competition of U_{hyp} and U_{max}, even though the hypercooling behavior is expected in the intermetallic liquids. In addition, the hypercooling behavior of the liquids occurs with different contributions of U_{hyp} and U_{max}. In other words, deep supercooling is not the only prerequisite for realizing hypercooling.

C. Hypercooling parameter (α_{hyp}) and glass forming ability

In the previous session, we revealed that a smaller $\Delta\rho_f$ produces a smaller U_{hyp}, significantly influencing the hypercooling behavior of liquids. If we can substantially reduce $\Delta\rho_f$ by mixing more elements having strong negative ΔH_{mix} and significant atomic size mismatch, the hypercooling behavior can be enforced further with a smaller ΔT_{hyp} ($= T_m - T'_{hyp}$) along the line B in Fig. 1. Consequently, the liquid can easily cool below T'_{hyp} and may become more viscous, thereby facilitating glass formation. It should be recalled that the small density difference between liquid and crystal has been found in the formation of binary [30], ternary [72], and multicomponent BMGs [21]. In fact, this is consistent with the dense packing criterion of glass formation for many BMGs [70,73]. Moreover, such mixing can also affect atomic mobility (i.e., slow diffusion, or high viscosity), which is one of the key factors governing glass formation [74,57]. In this regard, the hypercooling parameter (α_{hyp}) should be connected to GFA from both thermodynamic and kinetic viewpoints, which has never been explicitly elucidated.

We deduce the relation of hypercooling and GFA (i.e., T_{hyp}, T_g, and T_m) from Fig. 1(b). At T_m, the enthalpy of liquid is given by $H_L(T_m) = H_g(T_g) + C_{P,L}(T_m - T_g)$ and the specific heat is $C_{P,L} = \Delta H_f/\Delta T_{hyp}$. Then, the enthalpy difference between liquid and glass (i.e., $\Delta H_{Lg} = H_L(T_m) - H_g(T_g) = H_c(T_m) + \Delta H_f - H_g(T_g) = \Delta H_{cg} + \Delta H_f$) is given by

$$\Delta H_{Lg} = \Delta H_{cg} + \Delta H_f = \frac{T_m - T_g}{T_m - T_{hyp}}\Delta H_f = \frac{1 - T_{rg}}{U_{hyp}}\Delta H_f, \tag{4}$$

where T_{rg} is the Turnbull parameter ($T_{rg} = T_g/T_m$) [42]. After rearranging Eq. (4), U_{hyp} is expressed as

$$U_{hyp} = \frac{1 - T_{rg}}{\left(1 + \frac{\Delta H_{cg}}{\Delta H_f}\right)}. \tag{5}$$

Note that the hypercoolability (U_{hyp}) is now connected to one of the representative GFA parameters, T_{rg}. Since the value of the denominator in Eq. (5) is positive and greater than one, GFA increases with increasing T_{rg} and decreasing U_{hyp}. Although Fig. 1(b) is schematic and simplified, Eq. (5) explicitly exhibits the relation of hypercooling limit and GFA. It is worth mentioning that Eqs. (4) and (5) include T_{hyp}, T_g, T_m, and enthalpy difference between crystal and glass which have been used to develop GFA parameters [29].

We further scrutinize the relation of the hypercooling limit (or α_{hyp}) and GFA in BMGs from binary to multicomponent alloys. In Fig. 5(a), α_{hyp} increases overall with the critical thickness (D_{max}) of these BMGs, despite the uncertainty of D_{max} (see the comparison with other GFA parameters [42–46] in Table S4-5 and Fig. S5 in SM [37]). Slightly decreasing U_{max} of the BMGs with D_{max} cannot explain the tendency of GFA [Fig. 5(b)]. However, U_{hyp} distinctly decreases with GFA in overall, yielding the increasing α_{hyp}. This behavior indicates the strong impact of the hypercooling on glass formation, which is consistent with Eq. (5). Again, as the number of components having different atomic sizes increases, the difference in excess volume between liquid and crystal becomes smaller [21], making a small change of k_L. Therefore, the change of U_{hyp} (or ΔT_{hyp}) should be relatively small. Accordingly, $\Delta\rho_f$ plays the decisive role in U_{hyp} ($\propto \Delta\rho_f/k_L$) in multicomponent alloys [Fig. 5(c)] and thus in GFA.

We can understand the effect of hypercooling limit on GFA within the frame of CNT [68]. The nucleation rate per unit volume and unit time is given by

$$I = \frac{C}{\eta}\exp\left(-\frac{\Delta G^*}{k_B T}\right), \tag{6}$$

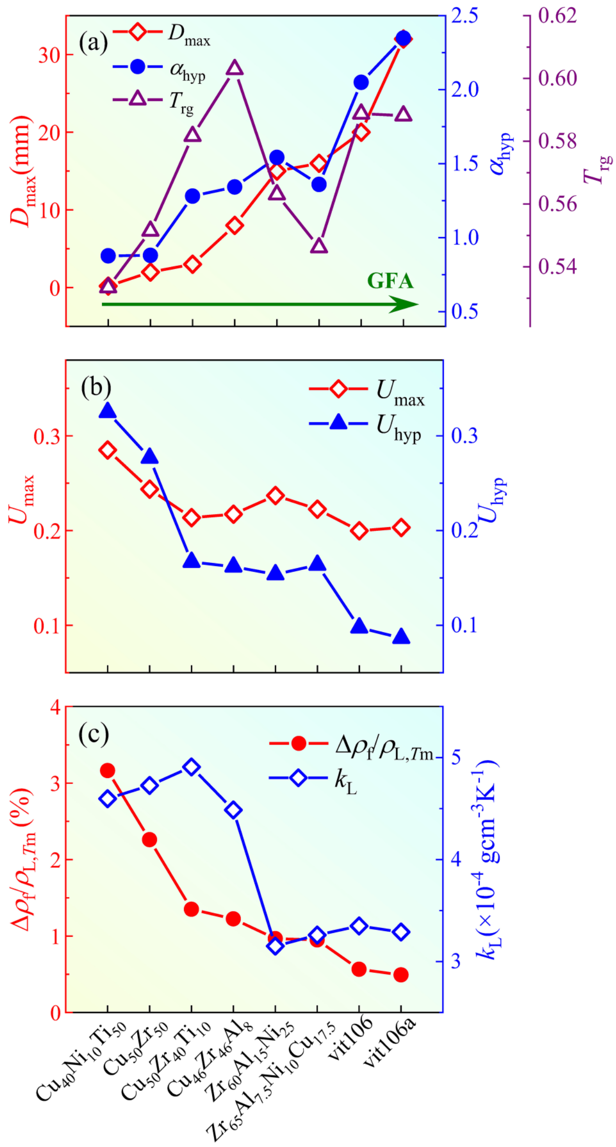

FIG. 5. The relation between hypercooling parameter α_{hyp} and GFA of various bulk metallic glasses. (a) D_{max} and α_{hyp} and T_{rg}; (b) U_{max} and U_{hyp}; (c) normalized $\Delta\rho_f$ ($\Delta\rho_f/\rho_{L,Tm}$, where $\rho_{L,Tm}$ is the liquid density at T_m) and k_L.

where C, ΔG^*, η, and k_B denote a constant, nucleation barrier, viscosity of liquid, and the Boltzmann constant, respectively. Assuming that at least one nucleus with the critical size is needed to initiate nucleation, $I \times V \times t$ should be greater than one at a given temperature and volume [68]. Then, the time t for nucleation in unit volume is given by

$$\ln t \propto \ln \eta + \frac{\Delta G^*}{k_B T}. \quad (7)$$

Thus, the time for the nucleation event is proportional to η and ΔG^*.

Previously, Mukherjee *et al.* [21] found that the viscosity (η_m) of liquids was proportional to $\exp(CV_{S,Tm}/\Delta V_f)$ (here, C is constant) for several pure metals, binary eutectics, and strong glass formers at T_m. The smaller ΔV_f (or $\Delta\rho_f$) is correlated to the excess volume of the liquid and thus gives the larger viscosity. This yields a longer time for the nucleation event in Eq. (7), which is consistent with the results in Fig. 5(c).

The other factor affecting the nucleation time is the nucleation barrier ΔG^* which is inversely proportional to $(\Delta H_f)^2$ (i.e., $\Delta G^* = 16\pi\sigma^3 T_m^2/3\Delta H_f^2\,\Delta T^2$). Here, ΔH_f is proportional to $\Delta\rho_f$ (i.e., $\Delta H_f = C_{P,L}\Delta T_{hyp} \propto C_{P,L}\Delta\rho_f/k_L$). Thus, the reduced $\Delta\rho_f$ by alloying can increase both the nucleation barrier ΔG^* and the liquid viscosity. This can cause a longer time for nucleation occurrence, which facilitates easier glass formation as temperature decreases. Since the smaller $\Delta\rho_f$ produces smaller ΔT_{hyp} in Eq. (2), the larger hypercooling parameter ($\alpha_{hyp} \sim 1/\Delta T_{hyp} \sim 1/\Delta\rho_f$) indicates the better GFA. It is worth emphasizing that this study reveals the relationship between the hypercooling limit and the glass formation in both kinetic and thermodynamic viewpoints.

IV. CONCLUSIONS

In the present study, we unveil the hidden role of hypercoolability U_{hyp} in supercooling behavior and glass formation from elemental to multicomponent liquids. We find that ETM liquids show hypercooling behavior due to the smaller density difference between liquid and crystal at the melting temperature than LTM liquids, although ETM liquids have smaller undercoolability U_{max} than LTM liquids. This explains the relatively easier glass formation of ETM liquids than LTM ones. Moreover, the hypercooling behavior of alloy liquids is determined by the combination of U_{max} and U_{hyp}, which can be described by a dimensionless parameter α_{hyp} ($= U_{max}/U_{hyp}$). This exhibits that large U_{max} is not the only necessary condition for the hypercooling behavior. Moreover, we find a clear relation between the hypercooling limit and GFA, which has been suspected [12], but not explicitly considered before. Thus, the hypercooling parameter α_{hyp} can be considered as one of the indicators of GFA. Furthermore, the present study clearly demonstrates that the impact of hypercooling extends to not only crystal growth but also glass formation. Accordingly, the findings in this study open a new way to manipulate the supercooling behavior and glass formation, which is of great importance in applications and should stimulate further studies in many research areas, including physics, chemistry, materials science, metallurgy, and biology.

ACKNOWLEDGMENTS

We thank Dr. Brillo for useful discussion and comments, and Dr. J. Lee for technical support. This research was supported by Characterization platform for advanced materials funded by Korea Research Institute of Standards and Science (KRISS-2024-GP2024-0014) and by the National Research Council of Science & Technology (NST) grant by the Korea government (MSIT) (No. CAP23041-100).

[1] D. Turnbull and R. E. Cech, Microscopic observation of the solidification of small metal droplets, J. Appl. Phys. **21**, 804 (1950).

[2] F. C. Frank, Supercooling of liquids, Proc. R. Soc. London A **215**, 43 (1952).

[3] F. Spaepen, A structural model for the solid-liquid interface in monatomic systems, Acta Metall. **23**, 729 (1975).

[4] M. H. Cohen and D. Turnbull, Molecular transport in liquids and glasses, J. Chem. Phys. **31**, 1164 (1959).

[5] G. Adam and J. H. Gibbs, On the temperature dependence of cooperative relaxation properties in glass-forming liquids, J. Chem. Phys. **43**, 139 (1965).

[6] M. Goldstein, Viscous liquids and the glass transition: A potential energy barrier picture, J. Chem. Phys. **51**, 3728 (1969).

[7] W. Gotze and L. Sjogren, Relaxation processes in supercooled liquids, Rep. Prog. Phys. **55**, 241 (1992).

[8] W. Kurz, B. Giovanola, and R. Trivedi, Theory of microstructural development during rapid solidification, Acta Metall. **34**, 823 (1986).

[9] H. S. Chen, Thermodynamic considerations on the formation and stability of metallic glasses, Acta Metall. **22**, 1505 (1974).

[10] H. W. Kui, A. L. Greer, and D. Turnbull, Formation of bulk metallic glass by fluxing, Appl. Phys. Lett. **45**, 615 (1984).

[11] M. E. Glicksman and R. J. Schaefer, Investigation of solid/liquid interface temperatures via isenthalpic solidification, J. Cryst. Growth. **1**, 297 (1967).

[12] P. Fopp, M. Kolbe, F. Kargl, R. Kobold, and W. Hornfeck, Unexpected behavior of the crystal growth velocity at the hypercooling limit, Phys. Rev. Mater. **4**, 073405 (2020).

[13] C. G. Levi and R. Mehrabian, Microstructures of rapidly solidified aluminum alloy submicron powders, Metall. Trans. A **13**, 13 (1982).

[14] S. Y. Lu, J. F. Li, and Y. H. Zhou, Grain refinement in the solidification of undercooled Ni-Pd alloys, J. Cryst. Growth **309**, 103 (2007).

[15] K. Nagashio and K. Kuribayashi, Rapid solidification of $Y_3Al_5O_{12}$ garnet from hypercooled melt, Acta Mater. **49**, 1947 (2001).

[16] K. Nagashima, K. Tsukamoto, H. Satoh, H. Kobatake, and P. Dold, Reproduction of chondrules from levitated, hypercooled melts, J. Cryst. Growth **293**, 193 (2006).

[17] C. C. Hays, J. Schroers, W. L. Johnson, T. J. Rathz, R. W. Hyers, J. R. Rogers, and M. B. Robinson, Vitrification and determination of the crystallization time scales of the bulk-metallic-glass-forming liquid $Zr_{58.5}Nb_{2.8}Cu_{15.6}Ni_{12.8}Al_{10.3}$, Appl. Phys. Lett. **79**, 1605 (2001).

[18] G. Shete, S. Mishra, S. Karagadde, and A. Srivastava, On the phenomena of partial crystallization of highly undercooled magnesium silicate molten droplets, Sci. Rep. **11**, 13666 (2021).

[19] Q. Wang, L.-M. Wang, M. Z. Ma, S. Binder, T. Volkmann, D. M. Herlach, J. S. Wang, Q. G. Xue, Y. J. Tian, and R. P. Liu, Diffusion-controlled crystal growth in deeply undercooled melt on approaching the glass transition, Phys. Rev. B **83**, 014202 (2011).

[20] C. Tang and P. Harrowell, Anomalously slow crystal growth of the glass-forming alloy CuZr, Nat. Mater. **12**, 507 (2013).

[21] S. Mukherjee, J. Schroers, Z. Zhou, W. L. Johnson, and W. K. Rhim, Viscosity and specific volume of bulk metallic glass-forming alloys and their correlation with glass forming ability, Acta Mater. **52**, 3689 (2004).

[22] J. Orava and A. L. Greer, Fast and slow crystal growth kinetics in glass-forming melts, J. Chem. Phys. **140**, 214504 (2014).

[23] D. H. Kang, S. Jeon, H. Yoo, T. Ishikawa, J. T. Okada, P. F. Paradis, and G. W. Lee, Nanosized nucleus-supercooled liquid interfacial free energy and thermophysical properties of early and late transition liquid metals, Cryst. Growth Des. **14**, 1103 (2014).

[24] S. Klein, D. Holland-Moritz, and D. M. Herlach, Crystal nucleation in undercooled liquid zirconium, Phys. Rev. B **80**, 212202 (2009).

[25] L. Zhong, J. Wang, H. Sheng, Z. Zhang, and S. X. Mao, Formation of monatomic metallic glasses through ultrafast liquid quenching, Nature (London) **512**, 177 (2014).

[26] J. A. N. Schroers, Glasses made from pure metals one cell at a time, Nature (London) **512**, 142 (2014).

[27] B. Vinet, L. Magnusson, H. Fredriksson, and P. J. Desré, Correlations between surface and interface energies with respect to crystal nucleation, J. Colloid Interface Sci. **255**, 363 (2002).

[28] T. H. Kim, A. K. Gangopadhyay, L. Q. Xing, G. W. Lee, Y. T. Shen, K. F. Kelton, A. I. Goldman, R. W. Hyers, and J. R. Rogers, Role of Ti in the formation of Zr-Ti-Cu-Ni-Al glasses, Appl. Phys. Lett. **87**, 1 (2005).

[29] C. Chattopadhyay, K. S. N. S. Idury, J. Bhatt, K. Mondal, and B. S. Murty, Critical evaluation of glass forming ability criteria, Mater. Sci. Technol. **32**, 380 (2016).

[30] Y. Li, Q. Guo, J. A. Kalb, and C. V. Thompson, Matching glass-forming ability with the density of the amorphous phase, Science **322**, 1816 (2008).

[31] L. Wang, Y. C. Cho, Y. Lee, J. J. Lee, and G. W. Lee, Density measurement and uncertainty evaluation of elemental and alloy liquids using electrostatic levitation, J. Mol. Liq. **396**, 123979 (2024).

[32] H. Yoo, C. Park, S. Jeon, S. Lee, and G. W. Lee, Uncertainty evaluation for density measurements of molten Ni, Zr, Nb and Hf by using a containerless method, Metrologia **52**, 677 (2015).

[33] S. Jeon, S. Ganorkar, Y. C. Cho, J. Lee, M. Kim, J. Lee, and G. W. Lee, Precise density measurement and its uncertainty evaluation for refractory liquid metals over 3000 K using electrostatic levitation, Metrologia **59**, 045008 (2022).

[34] *Smithells Metals Reference Book*, 7th ed., edited by E. A. Brandes and G. B. Brook (Butterworth-Heinemann, Oxford, 1998).

[35] D. M. Herlach, Non-equilibrium solidification of undercooled metallic melts, Mater. Sci. Eng. R **12**, 177 (1994).

[36] J. W. Arblaster, Thermodynamic properties of tantalum, J. Phase Equilibria Diffus. **39**, 255 (2018).

[37] See Supplemental Material at http://link.aps.org/supplemental/10.1103/PhysRevMaterials.8.063401 for the typical temperature profile and density behavior of all the twelve elemental transition metals; hypercooling limit $\Delta T_{\rm hyp}$ of transition metals determined by zero-plateau time (ZPT) method; density behavior and alloying effect on the supercooling behavior of binary alloys; and comparison of GFA and $\alpha_{\rm hyp}$ parameters on various bulk metallic glasses.

[38] A. Takeuchi and A. Inoue, Classification of bulk metallic glasses by atomic size difference, heat of mixing and period of constituent elements and its application to characterization of the main alloying element, Mater. Trans. **46**, 2817 (2005).

[39] S. Jeon, D. H. Kang, S. H. E. Kang, S. H. E. Kang, J. T. Okada, T. Ishikawa, S. Lee, and G. W. Lee, Non-contact measurement

of thermophysical properties of Fe, Fe-C, and Fe-C-Mn alloys in solid, supercooled, and stable liquid phases, ISIJ Int. **56**, 719 (2016).
[40] Y. C. Cho, B.-S. Kim, H. Yoo, J. Y. Kim, S. Lee, Y.-H. Lee, G. W. Lee, and S.-Y. Jeong, Successful melting and density measurements of Cu and Ag single crystals with an electrostatic levitation (ESL) system, CrystEngComm. **16**, 7575 (2014).
[41] B. J. A. Cahill, The density of liquid copper from its melting point (1356 K) to 2500 K and an estimate of its critical constants, J. Phys. Chem. **66**, 1080 (1961).
[42] D. Turnbull, Under what conditions can a glass be formed?, Contemp. Phys. **10**, 473 (1969).
[43] A. Inoue, T. Zhang, and T. Masumoto, Glass-forming ability of alloys, J. Non-Cryst. Solids **156–158**, 473 (1993).
[44] Z. P. Lu and C. T. Liu, Glass formation criterion for various glass-forming systems, Phys. Rev. Lett. **91**, 115505 (2003).
[45] K. Mondal and B. S. Murty, On the parameters to assess the glass forming ability of liquids, J. Non-Cryst. Solids **351**, 1366 (2005).
[46] S. Guo and C. T. Liu, New glass forming ability criterion derived from cooling consideration, Intermetallics **18**, 2065 (2010).
[47] C. Ma, H. Soejima, S. Ishihara, K. Amiya, N. Nishiyama, and A. Inoue, New Ti-based bulk glassy alloys with high glass-forming ability and superior mechanical properties, Mater. Trans. **45**, 3223 (2004).
[48] P. Yu, H. Y. Bai, and W. H. Wang, Superior glass-forming ability of CuZr alloys from minor additions, J. Mater. Res. **21**, 1674 (2006).
[49] H. Men, S. J. Pang, and T. Zhang, Glass-forming ability and mechanical properties of $Cu_{50}Zr_{50-x}Ti_x$ alloys, Mater. Sci. Eng. A **408**, 326 (2005).
[50] Q. S. Zhang, W. Zhang, and A. Inoue, Effects of addition of Al, Ti and Ag on glass-forming ability of $Cu_{50}Zr_{50}$ alloy, Mater. Sci. Forum. **561–565**, 1333 (2007).
[51] Q. Zhang, W. Zhang, G. Xie, and A. Inoue, Glass-forming ability and mechanical properties of the ternary Cu-Zr-Al and quaternary Cu-Zr-Al-Ag bulk metallic glasses, Mater. Trans. **48**, 1626 (2007).
[52] Y. H. Li, W. Zhang, C. Dong, J. B. Qiang, A. Makino, and A. Inoue, Formation and mechanical properties of Zr-Ni-Al glassy alloys with high glass-forming ability, Intermetallics **18**, 1851 (2010).
[53] S. Sato, E. Matsubara, S. Tanaka, M. Kimura, M. Imafuku, T. Zhang, and A. Inoue, *In situ* observation of structural evolution of $Zr_{60}Al_{15}Ni_{25}$ bulk metallic glass in the supercooled liquid region, High Temp. Mater. Process. **19**, 299 (2000).
[54] Q. S. Zhang, W. Zhang, X. M. Wang, Y. Yokoyama, K. Yubuta, and A. Inoue, Structure, thermal stability and mechanical properties of $Zr_{65}Al_{7.5}Ni_{10}Cu_{17.5}$ glassy alloy rod with a diameter of 16 mm produced by tilt casting, Mater. Trans. **49**, 2141 (2008).
[55] A. Inoue, T. Zhang, N. Nishiyama, K. Ohba, and T. Masumoto, Preparation of 16 mm diameter rod of amorphous $Zr_{65}Al_{7.5}Ni_{10}Cu_{17.5}$ alloy, Mater. Trans. JIM. **34**, 1234 (1993).
[56] W. Chen, Y. Wang, J. Qiang, and C. Dong, Bulk metallic glasses in the Zr-Al-Ni-Cu system, Acta Mater. **51**, 1899 (2003).
[57] W. L. Johnson, J. H. Na, and M. D. Demetriou, Quantifying the origin of metallic glass formation, Nat. Commun. **7**, 10313 (2016).
[58] C. C. Hays, J. Schroers, U. Geyer, S. Bossuyt, N. Stein, and W. L. Johnson, Glass forming ability in the Zr-Nb-Ni-Cu-Al bulk metallic glasses, Mater. Sci. Forum. **343**, 103 (2000).
[59] W. Dong, H. Zhang, W. Sun, B. Ding, and Z. Hu, Formation, thermal stability and mechanical properties of Zr-Nb-Cu-Ni-Al bulk metallic glasses, Mater. Trans. **47**, 1294 (2006).
[60] Y. J. Duan, D. S. Yang, J. C. Qiao, D. Crespo, J. M. Pelletier, L. Li, K. Gao, and T. Zhang, Relaxation of internal friction and shear viscosity in $Zr_{57}Nb_5Al_{10}Cu_{15.4}Ni_{12.6}$ metallic glass, Intermetallics **124**, 106846 (2020).
[61] I. Gallino, M. B. Shah, and R. Busch, Enthalpy relaxation and its relation to the thermodynamics and crystallization of the $Zr_{58.5}Cu_{15.6}Ni_{12.8}Al_{10.3}Nb_{2.8}$ bulk metallic glass-forming alloy, Acta Mater. **55**, 1367 (2007).
[62] S. Mukherjee, Z. Zhou, J. Schroers, W. L. Johnson, and W. K. Rhim, Overheating threshold and its effect on time-temperature-transformation diagrams of zirconium based bulk metallic glasses, Appl. Phys. Lett. **84**, 5010 (2004).
[63] G. W. Lee, S. Jeon, C. Park, and D. H. Kang, Crystal-liquid interfacial free energy and thermophysical properties of pure liquid Ti using electrostatic levitation: Hypercooling limit, specific heat, total hemispherical emissivity, density, and interfacial free energy, J. Chem. Thermodyn. **63**, 1 (2013).
[64] S. J. Yang, L. Hu, L. Wang, and B. Wei, Heterogeneous nucleation and dendritic growth within undercooled liquid niobium under electrostatic levitation condition, Chem. Phys. Lett. **684**, 316 (2017).
[65] M. Barth, F. Joo, B. Wei, and D. M. Herlach, Measurement of the enthalpy and specific heat of undercooled nickel and iron melts, J. Non-Cryst. Solids **156–158**, 398 (1993).
[66] G. Kaptay, A unified model for the cohesive enthalpy, critical temperature, surface tension and volume thermal expansion coefficient of liquid metals of bcc, fcc and hcp crystals, Mater. Sci. Eng. A **495**, 19 (2008).
[67] Y. Waseda and S. Tamaki, The structures of 3D-transition metals in the liquid state, Philos. Mag. **32**, 273 (1975).
[68] K. F. Kelton, Crystal nucleation in liquids and glasses, Solid State Phys. **45**, 75 (1991).
[69] O. N. Senkov and D. B. Miracle, Effect of the atomic size distribution on glass forming ability of amorphous metallic alloys, Mater. Res. Bull. **36**, 2183 (2001).
[70] A. Inoue, Stabilization of metallic supercooled liquid and bulk amorphous alloys, Acta Mater. **48**, 279 (2000).
[71] D. B. Miracle, W. S. Sanders, and O. N. Senkov, The influence of efficient atomic packing on the constitution of metallic glasses, Philos. Mag. **83**, 2409 (2003).
[72] Q. Guo, J. H. Noh, P. K. Liaw, P. D. Rack, Y. Li, and C. V. Thompson, Density change upon crystallization of amorphous Zr-Cu-Al thin films, Acta Mater. **58**, 3633 (2010).
[73] L. Yang, G. Q. Guo, L. Y. Chen, C. L. Huang, T. Ge, D. Chen, P. K. Liaw, K. Saksl, Y. Ren, Q. S. Zeng, B. Laqua, F. G. Chen, and J. Z. Jiang, Atomic-scale mechanisms of the glass-forming ability in metallic glasses, Phys. Rev. Lett. **109**, 105502 (2012).
[74] S. Mukherjee, W. L. Johnson, and W. K. Rhim, Noncontact measurement of high-temperature surface tension and viscosity of bulk metallic glass-forming alloys using the drop oscillation technique, Appl. Phys. Lett. **86**, 014104 (2005).